^{3}He(γ,np)p reaction in quasi-deuteron kinematics

N. R. Kolb,* P. N. Dezendorf,† M. K. Brussel, B. B. Ritchie, and J. H. Smith
Nuclear Physics Laboratory and Department of Physics, University of Illinois at Urbana–Champaign, Champaign, Illinois 61820
(Received 12 November 1990)

Coincident neutron-proton pairs were measured from the reaction ^{3}He(γ,np)p with a 100-MeV bremsstrahlung beam. The energy and angle of the neutron and proton were used to reconstruct the photon energy, making this a kinematically complete experiment. Quasi-deuteron breakup was observed for photon energies from 45 to 95 MeV. The angular distribution of the np pairs was measured for opening angles from 122 to 202 degrees in the laboratory frame. The single-differential cross section in Ω_p was determined at $\theta_p = 81°$, relative to deuterium, to range from 2.4 at 55 MeV to 1.7 at 95 MeV.

I. INTRODUCTION

Experiments on light nuclei with real photons have shown the importance of the quasi-deuteron effect for photon energies up to $\Delta(1232)$ resonance [1–10]. This experiment was designed to study the onset of quasi-deuteron breakup kinematics in ^{3}He.

Levinger [11] first postulated a photoabsorption mechanism in which an incident photon interacts with a np pair in the nucleus. He called these pairs quasi-deuterons since the two nucleons are ejected in kinematics similar to that seen from the breakup of a free deuteron. Microscopic calculations, such as those of Laget [12], are now able to treat the ^{3}He nucleus in a fundamental way by including meson-exchange currents (and hence the quasi-deuteron correlations) as well as final-state interactions. This makes ^{3}He an especially important system in which to study the inputs to the theory.

Barton and Smith measured coincident np pairs, in 1954, from natural helium and lithium, among other elements, using 280-MeV bremsstrahlung and were successful in identifying quasi-deuteron events [1]. In the same year, Myers detected quasi-deuterons from carbon and oxygen [2]. More recently, Wade found quasi-deuteron events from ^{6}Li for photons in the 35–65-MeV range with a 67-MeV bremsstrahlung beam [5]. Gorbunov noted that in ^{3}He the reaction for $E_\gamma \geq 75$ MeV is primarily quasi-deuteron [3], but had only $\sim$60 events in this region. In an experiment preliminary to the one reported here, Dezendorf also found evidence for quasi-deuteron breakup from ^{3}He [6], showing that the quasi-deuteron effect was clearly present for photon energies as low as 45 MeV, somewhat at odds with the qualitative observation of Gorbunov. Quasi-deuteron breakup has also been found to be important in a recent (e,$e'p$) experiment at Saclay [13].

II. EXPERIMENTAL TECHNIQUE

Coincident neutron-proton pairs were detected from the disintegration of ^{3}He in a 100-MeV bremsstrahlung photon beam incident on a cryogenic gas target. The particles were detected, on opposite sides of the beam, with scintillation counters. The neutron energy was obtained from its time of flight and the proton energy from a NaI crystal in which the protons were stopped. Complete details can be found in Ref. [7].

The bremsstrahlung photon beam was produced from an electron beam supplied by the 100% duty cycle microtron located at the Nuclear Physics Laboratory, University of Illinois, Urbana–Champaign.

Figure 1 shows the general arrangement of the experiment. The electron beam from the microtron was incident on a platinum radiator (0.013 radiation lengths) to produce the bremsstrahlung photons. The electrons were then deflected by a magnetic field out of the beam path and down to a graphite block which served as a Faraday cup used for a qualitative monitor. The photons passed through a set of collimators to form a circular spot 4.3 cm in diameter at the target. After passing through the scattering chamber the photons were incident on an ionization chamber of the P2 type [14]. This gave a measure of the photon-beam intensity and total energy with which the target was irradiated during the experiment and was used to normalize the data sets.

The neutron counter was a position-sensitive array of 12 long scintillators which had a phototube at either end. Each scintillator was $182.9 \times 15.2 \times 2.5$ cm^3 and the 12 were arranged one above the other into a nearly square array. It was located 401 cm from the target center to measure the time of flight of the neutrons and hence determine their energy. The neutron energy resolution varied from 2% at 10 MeV to 5% at 50 MeV (rms deviation). The position of a neutron hit on the counter determined the polar angle θ_n (with respect to the photon beam axis) and the azimuthal angle ϕ_n with errors of 1.5° and 0.64°, respectively (rms deviation when the neutron detector is at 81°). Between the neutron counter and the target were hung lead sheets totaling 2.5-cm thickness to reduce electromagnetic backgrounds from the target. The center of the lead was located 6.3 cm from the face of the detector.

The proton detector was of the dE-E type. The dE counter was a thin disc of plastic scintillator 0.025 cm thick and 5.1 cm in diameter, located 25.3 cm from the target center. It gave a measure of the energy loss of protons passing through it. The dE signal served as the reference time for measuring the time of flight of coin-

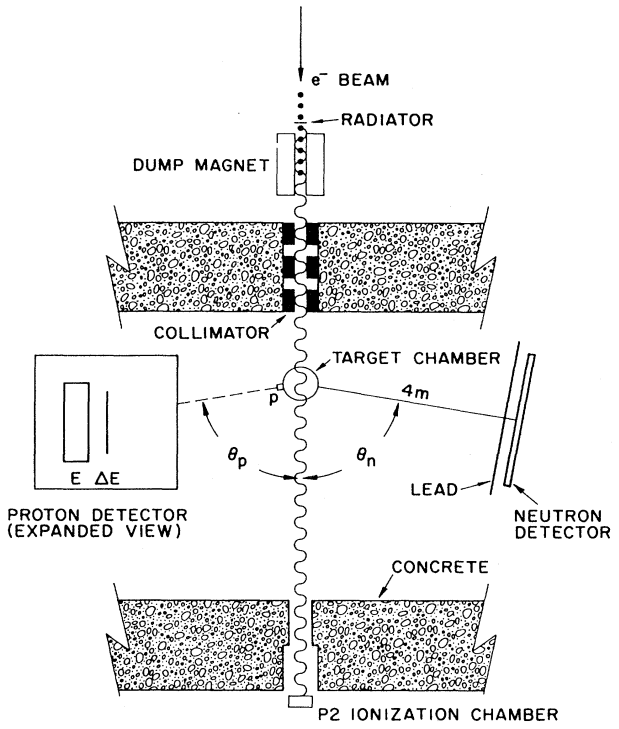

FIG. 1. Overview of the experimental setup (not to scale).

cident neutrons. The E counter was located directly behind the dE and consisted of a NaI crystal thick enough (2.5 cm) to stop the highest-energy protons in this experiment. It was large enough in diameter (6.9 cm) that all the protons which passed through the dE scintillator would enter and remain in the crystal with generous allowance for scattering. The combination of total energy and energy loss makes it possible to discriminate protons from the electrons entering the detector. The angle of the proton counter with respect to the photon beam direction was changed by rotating the entire scattering chamber. The angle of scattered protons was determined to within 3.8° rms deviation.

The target was a cryogenic system which kept the ^{3}He target gas at liquid-^{4}He temperature (4.2 K). The gas was contained in a vertical cylinder of aluminized Mylar, 0.005 cm thick, epoxied to a copper flange at the top and plugged with a copper disk at the bottom which had Si diodes embedded in it to measure the temperature. The pressure of the gas ($\sim$500 Torr) was measured with a Barocell. The gas pressure and temperature were monitored during the experiment to obtain the density of the target gas ($\sim$29 mg/cm^2).

The experiment was calibrated by measuring coincident neutron-proton pairs from the photodisintegration of deuterium. In this case the particles are exactly correlated in energy and angle and serve as a standard for our detection system.

The pulse heights from the proton E counter were first calibrated in energy with ^{2}H(γ,np). From the energy and angle of emission of the neutron, the energy of the proton was determined and compared to the proton pulse height. The error in this calibration procedure was approximately 2%.

The neutron efficiency, shown in Fig. 2 for one of the central detector elements, was mainly determined by measuring neutron-proton coincidences from the photodisintegration of deuterium and dividing by the yield of protons from the same reaction without the requirement of a neutron coincidence. Nearly all the protons from deuterium have an associated neutron which passes through the counter, except at the lowest photon energies. The fraction of neutrons that miss (14% at neutron energies of 12 MeV, $<$2% above 25 MeV and 0% above 30 MeV) was accurately determined by a Monte Carlo calculation. The neutrons pass primarily through the central six elements of the neutron counter array, leaving the outer counters untested. In addition, the neutrons pass through only a restricted region of the length of the central counters, these positions varying with neutron energy. These last two effects were alleviated by using a deuterium calibration target with a large proton counter and extended target region such that the neutron counter was bathed nearly uniformly with coincident neutrons. Deviations from uniformity were taken into account with a Monte Carlo calculation.

Neutron efficiencies were needed for neutron energies below the cutoff of the proton telescope (8.8 MeV for protons from deuterium). Consequently, the calibration target mentioned above was constructed with the proton scintillator directly in the deuterium gas. This carried the efficiency measurements down to neutron energies of 4 MeV. A few neutrons have energies below this, so the calibration was extended to 2 MeV with a californium source. The californium measurement covered the range of neutron energy from 2 to 7 MeV. In the region of overlap, the shape agreed with that from deuterium, but in magnitude was about 15% low. We believe the discrepancy was caused by scattering from an injudiciously placed Lucite holder. Consequently, the californium data were normalized to deuterium in the overlap region. The californium efficiency measurement affects

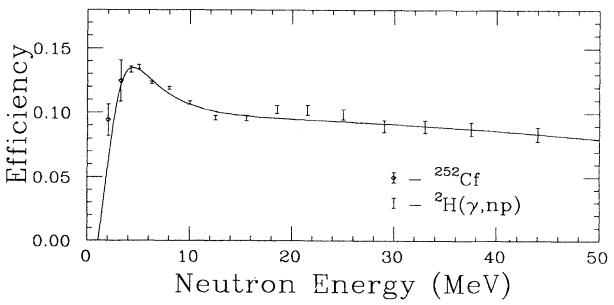

FIG. 2. Neutron efficiency for one of the scintillators. The lowest two points were measured with a ^{252}Cf source, the rest with deuterium photodisintegration.

only a small part of the data where the cross section is small, namely, transverse momenta greater than 230 MeV/c at 95 MeV in Fig. 3 and 130 MeV/c at 45 MeV.

Background subtractions were done to remove accidental coincidences between the proton and neutron counters. The density of such accidentals was taken from the unphysical time-of-flight region where no real coincidences could occur. This density of events was then subtracted across the time-of-flight spectrum.

The ^{3}He cross sections reported here were calculated by taking the ratio of the ^{3}He(γ,np) yields in each photon bin to the yields from ^{2}H(γ,p). These ratios were then scaled to μb by multiplying by the published cross sections of DePascale *et al.* [15].

The cross sections were corrected for events which were removed from their proper photon energy bin by the neutron being assigned an improper energy. The principal contribution to this effect was from interactions of neutrons in the lead in front of the detector producing low-energy neutrons with artificially long times of flight. For the proton energy calibration only, neutrons which scattered out of the deuterium kinematic locus were removed from consideration to minimize the effect of these slow neutrons. The photon energy in the two-body analysis of ^{2}H should be relatively unaffected since it is calculated from the proton energy. However, for ^{3}He this effect shifts some events into a lower photon energy bin.

The ^{2}H data determined what fraction of the neutrons were assigned energies which removed them from the proper photon energy bin. Both the neutron and proton were detected from ^{2}H photodisintegration, overdetermining the kinematics. The neutron energy was calculated from its time of flight (TOF) and independently from its associated proton's energy (from the pulse height) and angle. The neutron energy obtained from the proton data was unaffected by the TOF resolution. Comparing these two independent methods determined the total neutron energy resolution of the detector system. Errors in determining the neutron energy for ^{3}He can place an event in the wrong photon energy bin. The resolution function was used to generate a set of coupled equations, the solution of which described how to correct the number of detected events for each photon energy.

The cross section at a given angular setting of the counters was distributed over a range of neutron angles due to the large angular size of the neutron array. The angular half-width was 12.8° in θ_n and, near $\theta_n = 81°$, 13.4° in ϕ_n. To calculate the cross section at the central angles of the neutron detector, the distribution was fit with a quadratic at each angular setting of the counters, and for each photon energy bin. The factor by which to multiply the cross-section differential in transverse momentum (Sec. III) was determined by the ratio of the fit evaluated at the central angle to the average value of the distribution.

Table I lists the systematic errors in this experiment. Many possible systematic errors are eliminated or minimized by calculating our ^{3}He cross sections as ratios to deuterium. The calibration of the P2 chamber does not affect our cross sections, but it should be noted that it gave absolute cross sections for deuterium that were uniformly 10% below those of DePascale *et al.*, and therefore only a little outside the errors quoted for that compilation. For the bulk of our measurements the same target cell and manometer were used for deuterium and ^{3}He, and the temperatures were measured much better than the final statistical errors. Our data are presented and discussed in Sec. III, but here it should be noted that in the large peak near the center of each graph (Figs. 3 and 4) the kinematics of ^{3}He photodisintegration are so nearly

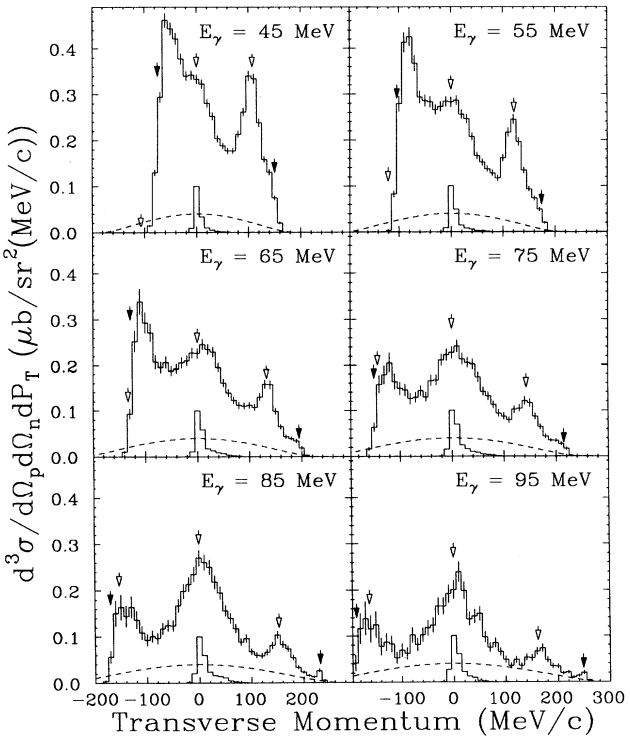

FIG. 3. ^{3}He(γ,np) differential cross section at $\theta_p/\theta_n = 81°/81°$ in the laboratory frame. From left to right, the filled arrows indicate the proton and neutron thresholds, and the open arrows the *PP*, QD, and *NP* locations. The dashed line represents phase space (unnormalized). The resolution from ^{2}H(γ,np) is indicated by the narrow histogram centered on zero.

TABLE I. Systematic error contributions in the present experiment.

Contribution	% error
Proton identification	2.0
Target thickness	2.6
Accidentals subtraction	3.0
DePascale normalization	3.2–10.0
Neutron efficiency	5.0–10.0

identical to those of deuterium that the neutron-counter efficiency effectively cancels from the cross-section calculation. Also, the effect of neutron scattering in the lead shield is nearly the same for ^{3}He and ^{2}H, so that the correction for scattering in the lead is made with complete confidence. Consequently, errors in our cross sections near the quasi-deuteron region should be mainly statistical with systematic errors related only to the cross sections DePascale *et al.* Toward the right of the graphs in Figs. 3 and 4, the cross sections are affected by uncertainties in the dependence of the neutron-counter efficiency on energy, a systematic error we estimate to be less than 7%. In this region the neutron is so slow that a substantial change in its energy by scattering in the lead shield would not affect the assignment of photon energy, so this correction is negligible. At the left of the graphs in Figs. 3 and 4, the cross sections are also affected by the energy dependence of the neutron-counter efficiency. For the highest-energy photons the neutron energy is so high its efficiency had to be extrapolated from the deuterium measurements. This might introduce a systematic error as large as 10%. Moreover, the neutron scattering in the lead is most important here, and to some degree it, too, must be extrapolated. This error might be as large as 20% in this region.

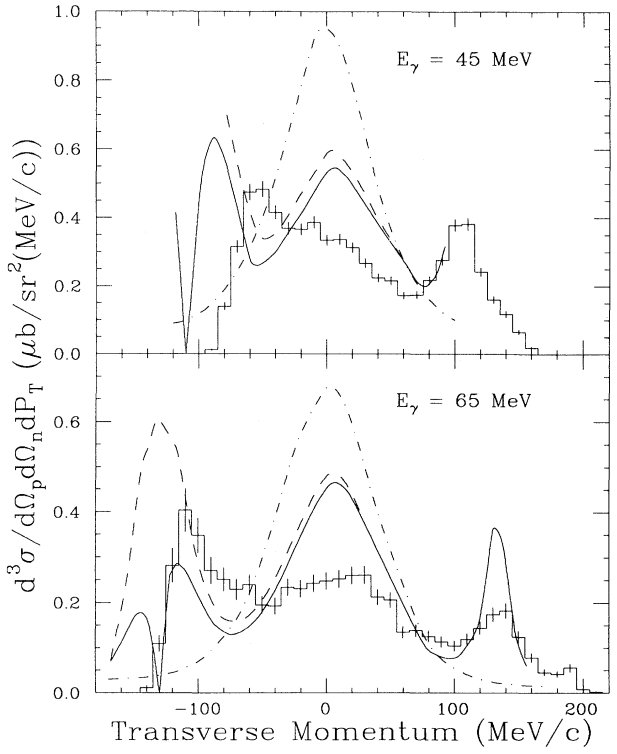

FIG. 4. ^{3}He(γ,np) differential cross section at $\theta_p/\theta_n = 84°/84°$ in the laboratory frame for photon energies of 45 and 65 MeV. The data are from the present experiment. The curves are calculations of Laget for plane wave (dot-dashed), distorted wave (dashed), and distorted wave with Coulomb (solid).

III. DISCUSSION AND RESULTS

Three final-state modes were seen in ^{3}He breakup: the *NP* final state in which the neutron and the undetected proton recoil together with nearly zero relative momentum, the *PP* final state where the detected and the undetected proton recoil with low relative momentum, and the quasi-deuteron (QD) final state in which the undetected proton is a spectator in the reaction and is left nearly at rest. In order to separate these it is useful to consider the momentum of the undetected proton transverse to the photon beam direction and in the horizontal plane through the center of the target. A positive value indicates the undetected proton was on the neutron-counter side of the beam, while for negative values it was on the proton-detector side. Values near zero correspond to the proton being left nearly at rest or moving parallel or antiparallel to the photon beam. If the neutron and proton are emitted at 90° in the center-of-mass system (CMS), which corresponds to about 81° in the laboratory for the upper photon energies of this experiment, then there is no longitudinal momentum and the spectator is left at rest.

Figure 3 shows the ^{3}He cross section for several photon energies at $\theta_p/\theta_n = 81°/81°$, differential in transverse momentum (P_T), and the proton (Ω_p) and neutron (Ω_n) solid angles. These data have been corrected for events removed from their proper photon energy (E_γ) bin by the neutron energy resolution. The error bars are due to the statistical uncertainties and the error associated with the neutron energy-resolution correction. The energy, in MeV, in the upper-right corner of the plots indicates the central energy of the photon bin. All photon bins are 10 MeV wide. The filled arrows are the transverse momentum cutoffs for the proton (left arrow) and the neutron (right arrow) detector thresholds. The proton threshold was 9.8 MeV from the ^{3}He target and the neutron threshold was set in the analysis as 1.7 MeV. The open arrows are, from left to right, the *PP* final-state point with zero relative momentum between the two protons, the quasi-deuteron (QD) breakup location at $P_T = 0$ with the undetected proton left at rest, and the *NP* final state in which the neutron and the undetected proton have zero relative momentum.

The dashed curves are a calculation of the phase space for the case where the neutron and proton are emitted at 90° in the CMS on opposite sides of the beam. The form of the curve is

$$\left[\frac{d^3\sigma}{d\Omega_p d\Omega_n dP_T}\right]_{\text{p.s.}} \propto \frac{[\frac{3}{4}(P_T^{\max})^2 - P_T^2]^2}{[(P_T^{\max})^2 - P_T^2]^{1/2}} , \tag{1}$$

where $P_T^{\max}$ is the maximum momentum that can be given to a single nucleon. The maximum energy is

$$E_{\max} \approx \tfrac{2}{3}(E_\gamma + E_b) , \tag{2}$$

where E_γ is the photon energy and E_b is the ^{3}He binding energy. $P_T^{\max}$ is then given by

$$P_T^{\max} = \left[\frac{4m}{3}(E_\gamma + E_b)\right]^{1/2} , \tag{3}$$

where m is the nucleon mass. These curves are not normalized but serve to illustrate that the transverse momentum plots have structures not described by phase space.

The experimental resolutions for P_T, the narrow histograms centered at zero, are shown for each photon bin. These are from an analysis of the ^{2}H coincidence data in which the deuteron is assumed to be a ^{3}He nucleus with -2.2-MeV binding energy. If the resolution were perfect these would be spikes at zero. The photon energy bins have been chosen to account for the 5.5-MeV difference in the binding energy of ^{2}H and ^{3}He. The width of the main peak is mostly from neutron time-of-flight errors. The prominent tail toward positive transverse momentum is from inelastic neutron interactions in the lead shielding in front of the neutron detector. The original neutron can interact in the lead and produce secondary, slower neutrons. The major effect of the resolution was to shift the transverse momentum peaks to slightly higher values, but only by ≤ 10 MeV/c. The data have not been corrected for this shift, but this small shift is just visible in the central peak at higher energies.

If the initial np pair with which the photon interacts is in motion in the nucleus, then the spectator proton will be left with some momentum. The width of the transverse momentum peak centered at zero is a measure of the momentum distribution of this proton in the ^{3}He nucleus. Final-state interactions and phase-space contributions affect the quasi-deuteron peak and distort this distribution. In the absence of any theoretical recipe the central QD peaks for $E_\gamma > 60$ MeV (Fig. 3) were fit with Gaussians centered at zero for the 81°/81° setting. The fitted width includes the resolution of the apparatus. To remove this, the ^{2}H peaks were fit with Gaussians and the widths subtracted in quadrature from the ^{3}He widths. The Gaussian rms width thus obtained, averaged over the photon energy bins, was 49.2 ± 3.0 MeV/c. The error quoted is the rms deviation.

A ^{3}He(e,$e'p$) experiment reported by Jans *et al.* [16] measured the proton momentum distribution for the two- and three-body breakup. The width of the quasi-deuteron peak reflects the momentum of the undetected proton in the (γ,np) reaction. This is probably best described by the sum of the two- and three-body breakup momentum densities of Jans. Fitting the Jans distribution from 15 to 95 MeV/c with a Gaussian (mean fixed at zero) yields a rms width of 46.5 ± 1.4 MeV/c. This is within the error of the value measured in this experiment.

Figure 4 shows a comparison of the present experiment to calculations of Laget [17] made in the framework of Ref. [12]. The dot-dashed curves are done with a plane wave in the final state, the dashed curves a distorted wave, and the solid curves the distorted wave with Coulomb effects. The addition of S-wave final-state interactions in the distorted-wave calculation reduces the strength in the quasi-deuteron region and forms the NP and PP final states in qualitative agreement with the data. Including Coulomb effects forces the cross section to zero at the position of zero relative momentum between the protons since the Coulomb repulsion forbids their relative energy to be zero. At the quasi-deuteron peak, the calculation is a factor of 1.6 to 1.8 above the experimental data, while in the PP final-state region the data are consistently high. This may indicate the need for higher partial waves in the NN rescattering series to shift more strength from the quasi-deuteron to the PP region.

The preliminary experiment of Dezendorf [6] at a lower peak bremsstrahlung energy of 67 MeV agrees with this one near the NP point, falls about 20% near the QD point, and is nearly a factor of 2 lower at the PP point. Those data were collected with a very different neutron counter with a thicker lead shield used at a smaller distance from the target. They were not corrected for neutron scattering in the lead shield, so this trend is what would be expected. In other ways those data agree very well with the data from this experiment.

The angular dependence of the ^{3}He cross sections is displayed in terms of the opening angle between the detected neutron and the detected proton (Fig. 5). The cross sections were adjusted to account for the angular distribution in ϕ_n across the counter. This was done by fitting the ϕ_n distribution with a quadratic for each angular setting of the counters. The result is cross sections at five opening angles, corresponding to the five neutron angular bins across the counter, for each of the detectors. Figure 5 shows the opening angle distribution for the ^{3}He data, where no attempt has been made to separate the

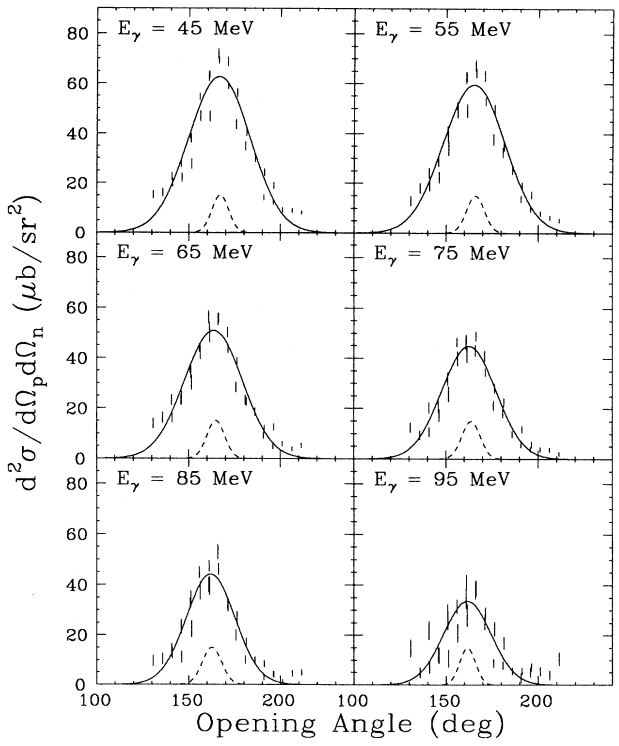

FIG. 5. ^{3}He(γ,np) differential cross section as a function of the opening angle between the neutron and proton for $\theta_p = 81°$ in the laboratory frame. The solid curve is a Gaussian fit. The angular resolution from ^{2}H(γ,np) is indicated by the dashed curve.

cross section into different final states. All the data except for five points from $\theta_p/\theta_n = 101°/101°$ were taken with the proton detector at 81°. Therefore, Fig. 5 describes the angular distribution of neutrons whose correlated proton is emitted at 81°. The solid curves are Gaussians fit to the data and are used to integrate over the neutron angular distribution. The dashed curves show the angular resolution of the experiment, measured with deuterium.

Data were also taken over a similar range of opening angles with the detectors at equal angles on opposite sides of the photon beam. The resulting angular distributions agreed with those displayed in Fig. 5 within the experimental errors [7].

The single differential cross section in $d\Omega_p$ was calculated by taking the ϕ_n and θ_n dependence to be the same. This was checked by comparing the distributions at $\theta_p/\theta_n = 81°/81°$ and found to be a valid assumption. Integration of the Gaussian in both θ_n and ϕ_n yields

$$d\sigma/d\Omega_p = 2\pi w^2 N_0 \ , \tag{4}$$

where w and N_0 are the width and amplitude of the fitted Gaussians (Fig. 5). The shape of the angular distribution is primarily due to the initial momentum distribution of the nucleons. However, the proton momentum distribution of Jans is not perfectly represented by a Gaussian. The error introduced by the above procedure was estimated by taking the ratio of the area under the Jans data and the integral of a Gaussian fit to the Jans data. This yields a value of $F_p = 1.06 \pm 0.05$, where the error is from the uncertainty in the Jans data and from the Gaussian fit. This introduces a small error in integrating over the angular distributions of Fig. 5 which is corrected for by multiplying the cross sections obtained from Eq. (4) by F_p^2. The calculated cross sections are displayed in Table II. The errors listed for the cross sections are from the fitted parameters. The ^{2}H cross sections from DePascale [15] are listed in Table II and are evaluated at the photon energy (E_γ) listed in column 1.

The ratio of the ^{3}He single-differential cross section ($d\sigma/d\Omega_p$) at $\theta_p = 81°$ to the deuterium cross section is given in Table II as a function of photon energy. The 45- and 55-MeV cross sections are low due to the proton threshold, which is above the *PP* final-state point for these energies, as shown in Fig. 3. These points should be raised by $\sim 10\%$ at 45 MeV, less at 55 MeV.

The quasi-deuteron cross section was estimated by integrating over transverse momentum from -65 to 95 MeV/c for photon energies above 60 MeV (Fig. 3). The single-differential cross section was then obtained via the prescription described in the preceding paragraphs. Table II lists the ratio of these quasi-deuteron cross sections to deuterium. It should be emphasized that this is a rough separation done in the absence of more refined theoretical techniques.

TABLE II. Single differential cross sections for ^{3}He(γ,p)np, from the measured coincidence data, at $\theta_p = 81°$ in the laboratory frame. The published ^{2}H values, from DePascale, are included for comparison. Column 5 is a rough estimate of the quasi-deuteron contribution (see text).

E_γ (MeV)	$d\sigma/d\Omega_p$ (μb/sr)			
	^{3}He	^{2}H	^{3}He/^{2}H	QD/^{2}H
45	38.0(±2.1)	20.1(±0.8)	1.89(±0.13)	
55	35.6(±1.7)	14.9(±0.7)	2.39(±0.16)	
65	27.2(±1.5)	11.7(±0.7)	2.32(±0.19)	1.21(±0.07)
75	20.8(±1.1)	9.7(±0.7)	2.14(±0.19)	1.06(±0.06)
85	16.8(±1.2)	8.3(±0.7)	2.02(±0.22)	0.96(±0.07)
95	12.2(±1.6)	7.3(±0.7)	1.67(±0.27)	0.59(±0.10)

IV. SUMMARY AND CONCLUSIONS

The presence of quasi-deuteron breakup kinematics was clearly indicated in the present experiment for photon energies as low as 55 MeV. It is less clear, but visible, even at 45 MeV (Fig. 3). This conflicts with Gorbunov's results in which no evidence of quasi-deuteron breakup was seen below 75 MeV [3]. The discrepancy can probably be attributed to the low statistics of that experiment and the difficulty of detecting, in a cloud chamber, the very-low-energy proton which was the spectator in the reaction. Laget's calculation of the transverse momentum cross sections [17] are a factor of 1.6–1.8 above the experimental results at the quasi-deuteron peak (Fig. 4). In the *PP* region the calculation is significantly below the data. This could be indicative of more strength being shifted from the quasi-deuteron to the *PP* final states by the final-state interactions than the calculation predicts. At higher photon energies Laget's calculations agree well with the experimental data of d'Hose *et al.* [10].

The overlap of the strong final-state-interaction peaks with the quasi-deuteron peak makes it impossible to separate reliably the quasi-deuteron contribution to the cross section experimentally. In this photon energy range, theoretical calculations which include the final-state interactions are required.

The highest photon bin of this experiment, 90–100 MeV, is dominated by the quasi-deuteron peak on the transverse momentum plots (Fig. 3). If the reaction mechanism is assumed to be entirely quasi-deuteron including the final-state-interaction peaks, then the number of quasi-deuterons is 1.67±0.27 (Table II). This agrees with the higher-energy result of d'Hose *et al.* [10] of 1.68±0.07.

This material is based upon work supported in part by the National Science Foundation under Grant No. NSF PHY 86-10493.

*Current address: Dept. of Physics, University of Alberta, Edmonton, Canada T6G 2N5.

†Current address: Center for Naval Analyses, 4401 Ford Ave., Alexandria, VA 22302.

[1] M. Q. Barton and J. H. Smith, Phys. Rev. **95**, 573 (1954); **110**, 1143 (1958).

[2] H. Myers, A. Odian, P. C. Stein, and A. Wattenberg, Phys. Rev. **95**, 573 (1954).

[3] A. N. Gorbunov, Tr. Fiz. Inst. Akad. Nauk SSSR **71**, 1 (1974).
[4] S. Homma *et al.*, Phys. Rev. Lett. **27**, 2536 (1984).
[5] M. W. Wade, M. K. Brussel, L. J. Koester, Jr., and J. H. Smith, Phys. Rev. Lett. **53**, 2540 (1984).
[6] P. N. Dezendorf, Ph.D. thesis, University of Illinois, 1986.
[7] N. R. Kolb, Ph.D. thesis, University of Illinois, 1990.
[8] S. N. Dancer *et al.*, Phys. Rev. Lett. **61**, 1170 (1988).
[9] P. D. Harty *et al.*, Phys. Rev. C **37**, 13 (1988).
[10] N. d'Hose *et al.*, Phys. Rev. Lett. **63**, 856 (1989).
[11] J. S. Levinger, Phys. Rev. **84**, 43 (1951); *Nuclear Photo-Disintegration* (Oxford University, New York, 1960).
[12] J. M. Laget, Phys. Lett. **151B**, 325 (1985); J. Phys. G **14**, 1445 (1988); in *New Vistas in Electro-Nuclear Physics*, edited by E. L. Tomusiak, H. S. Caplan, and E. T. Dressler (Plenum, New York, 1986), p. 361.
[13] C. Marchand *et al.*, Phys. Rev. Lett. **60**, 1703 (1988).
[14] J. S. Pruitt and S. R. Domen, Natl. Bur. Stand. (U.S.) Circ. No. 48 (U.S. GPO, Washington, D.C., 1962).
[15] M. P. DePascale *et al.*, Phys. Lett. **119B**, 30 (1982).
[16] E. Jans *et al.*, Nucl. Phys. **A475**, 687 (1987).
[17] J. M. Laget, private communication (1987).